Frequency Control Strategy for Grid-tied Virtual Power Plant Using SSA-tuned Fractional Order PID Controller

Abishek R, Dulal Chandra Das, Ashtabhuj Kumar Srivastava & Abdul Latif

Published online: 16 Mar 2023.

Submit your article to this journal 🗗

View related articles 🗗

View Crossmark data 🗗

RESEARCH ARTICLE

Check for updates

Frequency Control Strategy for Grid-tied Virtual Power Plant Using SSA-tuned Fractional Order PID Controller

Abishek R [1], Dulal Chandra Das [1], Ashtabhuj Kumar Srivastava [2] and Abdul Latif [3]

[1]Department of Electrical Engineering, National Institute of Technology Silchar, Silchar, Assam, India; [2]Department of Electrical Engineering, Indian Institute of Technology Roorkee, Roorkee, Uttarakhand, India; [3]Advanced Power & Energy Center, EECS Department, Khalifa University, Abu Dhabi, United Arab Emirates

ABSTRACT

This paper investigates the frequency control strategy of the Virtual Power Plant (VPP), with the structure of an independent control area that includes diverse Distributed Energy Resources. The proposed VPP system comprises generating units such as Solar PV, Archimedes Wave Energy Conversion, Biodiesel driven Generator, and Plug-in Hybrid Electric Vehicle, which are interconnected to conventional thermal power plant. Centralized control strategy is adopted for frequency control studies, by considering the communication time delays. Fractional order Proportional Integral Derivative (FOPID), Proportional Integral Derivative (PID), and Proportional Integral (PI) controllers are employed to perform the control action on generating units to perform the frequency control. Tuning of the controllers is done using optimization algorithms such as Particle Swarm Optimization, Firefly Algorithm, Grasshopper Optimization Algorithm, Ant Lion Optimizer, Sine Cosine Algorithm, and Salp Swarm Algorithm (SSA). By comparative analysis, SSA algorithm is proved to outperform the other algorithms in terms of minimizing the objective function of Integral of Squared Error of the deviations in system frequencies and tie-line power. The system is also investigated under various scenarios of generation and load disturbances to study the comparative performance of the FOPID controller over PID and PI controllers. Results prove the superiority of SSA-tuned FOPID controller over PID and PI controllers in terms of providing better system responses. Sensitivity test has been conducted on the system without resetting nominal controller gain values and the proposed SSA-tuned FOPID controller is proved to be robust against the uncertainties in the load and parameters of our system.

1. INTRODUCTION

Power quality is one of the main objectives of the power system operation. It mainly concerns maintaining the quality of voltage, waveform, and frequency of the supply power within the specified limits. The grid frequency is correlated with the active power balance in the grid. In modern power systems supplying a large number of consumers, the active power demand keeps on varying, creating frequency fluctuations in the grid. To maintain constant frequency in the grid, there should always be a balance between generated and consumed power. Automatic Load Frequency Control (ALFC) plays a significant role in maintaining this balance. ALFC senses the frequency deviation in the grid and initiates the control signals to the generating units to maintain the total generation level same as the demand. For interconnected power systems, the functionality of ALFC is to sustain both the deviations in frequency and tie-line power flow from its scheduled power flow level, which was committed based on the electricity market [1–3].

Over time, the structure of the power system changes very rapidly. Environmental concerns such as rising pollution levels, changes in climatic conditions, and the limited availability of conventional energy resources increasingly alarmed us to move towards the renewable source of electric power generation [4]. These factors motivate us to think about the new power system structure called Distributed Generation (DG), where the small-scale renewable generation technologies or conventional generation technologies with less-emission, high-efficient nature are installed near the customers' location in the distribution network [5,6]. Initially, the interconnection of DG to the distribution network is implemented using the "fit and forget" approach [7]. Those passively interconnected DGs in the distribution network faced technical and operational issues because of the uncertain nature of the interconnected RES [5,6]. The active control of the distribution network which can able to tackle these issues is implemented using the flexible nature of components in the distribution network. The flexibility and the control

capability required for the active control are respectively provided by the Distributed Energy Resources (DERs) and smart grid technologies such as smart metering, and Advanced Metering Infrastructure (AMI) [8]. The DERs include controllable DG technologies, distributed Energy Storage Systems (ESS) such as the battery, flywheel storage systems, electric vehicles employed with V2G configuration, and Demand Response (DR) programs [9]. Active control of distribution networks using DERs takes different topology forms, each having its own advantages and limitations [9,10]. Microgrids are one such kind of active distribution network that exploits the DERs, effectively [10].

Even with such effective integration of DERs either separately or in the form of microgrids, the need for Conventional Power Plant (CPP) is still unavoidable. It is because the DERs integration replaces the energy requirement of the CPPs but not its capacity [11]. Ancillary services, which are the support and security services required for the grid's proper operation, are still provided by the CPPs. The ancillary services primarily include fault-ride through, frequency control, voltage control, and congestion management [12]. The DERs installed separately or within the microgrids can supply these ancillary services. However, its small-scale capacity and the control structure limit the provision of its ancillary services only within the respective power delivery area. Thus the higher-level network like transmission network cannot benefit from the ancillary services capacity of DERs due to its small-scale and distributed nature [12]. Thus, the aggregation of the DERs within the network as a single large entity and increasing its visibility to the higher-level network controllers such as Transmission System Operator (TSO) effectively increases the exploitation of the benefits of the DERs [13]. This aggregation and increased visibility of the DERs are provided by the Virtual Power Plant framework [11,13]. The role of VPP is to find the operational characteristics of different DERs within its area, its technical and operational limits, and the network constraints within the VPP and then aggregate it to represent the single operational characteristics to the TSO as a CPP [11,13]. To perform the aggregation and control of DERs in the VPP, Information and Communication Technologies (ICT) take a significant place [12]. The DERs in the VPP need not to be in the same distribution network or the same geographical area. It can aggregate the distant DERs in the different networks covering a large geographical area [12]. And also, the VPP may be a single DER or aggregation of distant DERs, single microgrid or combination of microgrids enabled with VPP control structure [14]. Our study focuses on the VPP, with the structure

of an independent control area that aggregates diverse DERs.

As the VPP aggregates the DERs mainly to explore the provision of its ancillary services, its capability of frequency control support to the transmission network needs to be addressed. Literature survey reveals that several studies have been performed on ALFC of multi-area conventional power systems [15–18], isolated hybrid power systems [19–22], and interconnected microgrids [23–25], in order to sustain the frequency and tie-line power deviations. The primary motivation behind these works is to find a control strategy with a higher degree of reliability and faster response rates to meet the stringent quality requirements of the modern power system. Thus, the controllers such as PI, PID [15–21,23,24,26], Fractional order PID [25], H-infinity based [22] controllers have been employed. To obtain the optimal gains of the controllers, several meta-heuristic techniques like Genetic Algorithm [20], Particle Swarm Optimization [15], Biogeography based optimization [21], Artificial Bee colony algorithm [16], Teaching Learning-based optimization [17], Quasi Oppositional Harmony Search algorithm [26], Water Cycle Algorithm [18], Social Spider Optimizer [23], Firefly Algorithm [24], Butterfly Optimization algorithm [25] have been implemented.

It is to be noted that Energy Management System (EMS) is the heart of the VPP [27]. The functionalities of VPP are to obtain the forecast of renewable energy sources, needs of the customers of flexible loads and forecast of market prices to schedule the components of VPP for energy and ancillary services provision [27]. The optimization algorithms are implemented in EMS to maximize the profit, minimize the losses and minimize the cost of generation considering the technical and economical constraints of the VPP components [27,28]. This optimization and bidding in the EMS are done on day-ahead basis [29]. The scheduling results obtained after the market clearance are set for each DERs in the EMS and used for real-time interface and control processes [29]. VPP can be classified into two types based on its operational features as Commercial VPP (CVPP) and Technical VPP (TVPP) [29,30]. CVPP prepares the optimal schedule of DERs for market participation by obtaining the load forecasts, market price forecast, and other operational parameters of DERs [29,30]. TVPP collects the technical parameters of the DERs, real-time network constraints, and the optimal schedule from CVPP [29,30]. From the collected inputs, the aggregated VPP capabilities are computed and submitted to transmission or distribution network operators to increase the visibility of DERs for providing services to the grid [29,30].

During real-time generation and load disturbances, the EMS sends the control signal to the DER units according to the scheduled reserve capacities based on the market results [30]. In this regard, EMS uses the communication network to obtain the current status of each DERs and to transfer the control signal from EMS to DERs in the VPP system [27]. Thus, mathematical model representing this bi-directional communication delay should be included to simulate the real-time frequency control operation in VPP systems. As our work focuses on implementing the technical VPP to supply energy services to the grid network, the market structure is not discussed in our study. However, only a few works have been done on the frequency regulation support provision by VPP. It is evident in the studies [31–34] that the VPP can extend its ancillary service support of frequency regulation to the grid if there is any contingency. The primary level frequency support can be provided by observing the frequency drop and the control signals are initiated to DERs within the VPP to adjust the generation, when there is any contingency like faults in the transmission lines [31,34,35]. The secondary level frequency control can be carried out on the VPP of the independent control area, which has been executed in the work [36], using the Model Predictive Controller to sustain the frequency of the VPP system. The ALFC study on VPP system, which acts as an independent control area has been reported in the works [37,38]. The RESs such as Wind energy [37,38], Central receiver solar thermal system (CRSTS) [37], Parabolic-trough solar thermal system [38], and storage units like PHEV [37,38] have been integrated to the VPP in these studies. The same strategy as the interconnected micro-grids has been followed considering the communication delays [37,38]. To perform control action, the PI, PID [37], and the dual-stage PI-$(1 + PD)$ [38] controllers have been implemented. However, the more flexible and robust fractional order PID controller (FOPID) has never been explored in the ALFC study of the grid-tied VPP system in the literature. And also regarding the generating units, the RESs such as Ocean wave energy conversion and dispatchable Bio-diesel based generators have not yet been integrated in the grid-tied VPP model. Thus, the present work aims to bridge the research gap mentioned above.

1.1 Detailed Contributions of the Present Work

(1) To develop the transfer function model of Solar PV-Archimedes Wave Energy Conversion (AWEC)-Biodiesel driven Generator (BDDG)-Plug-in Hybrid Electric Vehicle (PHEV) based virtual power plant integrated with the conventional grid of reheat type thermal power plant.

(2) To obtain the optimal control parameters of FOPID controllers by minimizing the ISE performance index using different optimization techniques such as PSO, FA, GOA, ALO, SCA, and SSA and then evaluate their performance to find the optimal algorithm for the proposed model.

(3) To study the dynamic response of our system employed with FOPID, PID, and PI controllers, tuned by the Salp Swarm Algorithm (SSA) and then evaluate their performance to find the optimal controller.

(4) To perform sensitivity analysis of proposed SSA-tuned FOPID controllers by considering the uncertainties such as variations in loading conditions and parameters such as synchronizing tie line coefficient (T12) and frequency bias factors (B2) in the proposed grid-integrated VPP model.

1.2 Organization of the Paper

The rest of the paper is organized as follows. The mathematical modeling of the DER units used in the system is described in section 2. Section 3 discusses the objective function and the control methodology adopted in our work. Section 4 addresses the simulation results of the comparison of optimization techniques, comparison of controllers, and sensitivity test of the system. Results are concluded in section 5.

2. MODELING OF PROPOSED GRID-TIED VPP

The schematic of the proposed grid-tied VPP system is presented in Figure 1. System nomenclature and the values are presented in Table 1. Working functionalities and the mathematical modeling of the DER units employed in the proposed system are described in the following subsections.

2.1 Solar PV

Solar PV is advantageous in various aspects such as less maintenance, no moving parts, no noise, and its energy conversion process is environment-friendly [26]. The electrical power output from the solar PV primarily depends on levels of solar irradiance and temperature [23]. The solar PV system is always installed with Maximum Power Point Trackers (MPPT), which provides the maximum power at the output by adjusting the operating point in the P-V curve. The mathematical equation governing the electrical power output of solar PV is represented as [26],

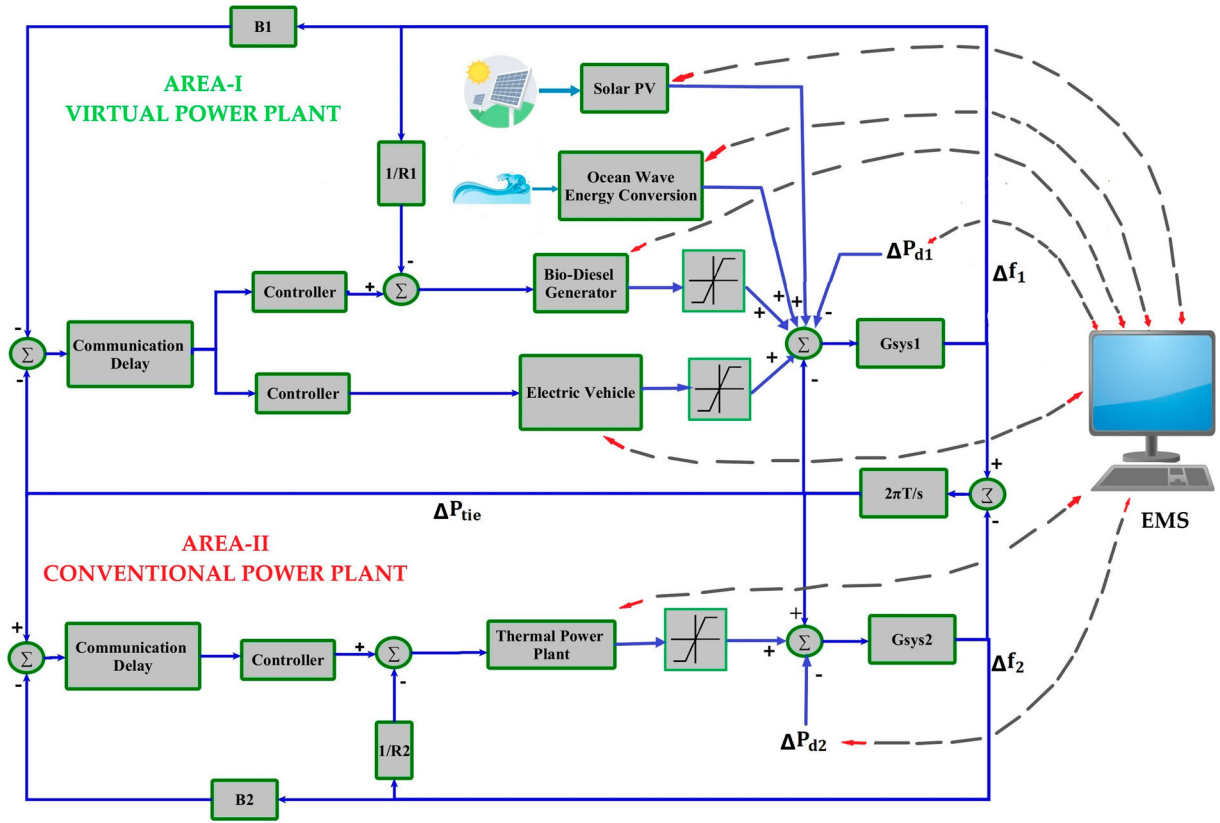$$P_{PV} = A\eta\{1 - (T_a + 25)0.005\}\Psi \qquad (1)$$

Figure 1: Schematic for proposed grid-tied VPP system

where A and η represent the surface area (m^2) and conversion efficiency (%) of the module, respectively. Ψ and T_a represent the solar irradiance (W/m^2) and ambient temperature (°C), respectively. In our study, the first-order linear transfer function model of the PV system is adopted and expressed as [26],

$$G_{PV} = \frac{K_{PV}}{1 + sT_{PV}} \tag{2}$$

2.2 Archimedes Wave Energy Conversion

The research interest in tapping the wave energy in oceans is developing because of its high energy density nature. Several technologies are existing for wave energy conversion, and AWEC is the more extensively implemented, which has not yet been explored in VPP. The Archimedes Wave Swing (AWS) floater on the ocean experiences vertical motion due to the waves, and the linear motion is transferred to the generator by the fixed bottom part at the sea bottom. To extract electrical power from the linear motion of the waves, the linear permanent magnet synchronous generator (LPMSG) is used [40].

The motion of the AWS can be expressed as [40],

$$V_f = \frac{dx}{dt} \tag{3}$$

$$F_{AWS} = m_{tm}\frac{dV_f}{dt} + \beta_{gd}V_f + \beta_{\omega d}V_f + k_t \tag{4}$$

where m_{tm} represents the total mass (kg), V_f represents the speed of the generator translator and floater (m/s), x represents the displacement of the generator translator and floater (m), β_{gd} and $\beta_{\omega d}$ represent the damping parameters of generator and wave swing (N s/m), respectively. k_t denotes the constant spring parameter (N/m). F_{AWS} represents the force experienced by the floater (N) of AWEC due to waves. Under irregular scenarios of ocean waves, the force that acts on the floater can be represented as [41],

$$F_{AWS} = F\sin(\omega_{AW}t) + \frac{F}{2}\sin(2\omega_{AW}t) + \frac{F}{3}\sin(3\omega_{AW}t) \tag{5}$$

where F represents the magnitude (N), ω_{AW} represents the angular frequency (rad/s) of forces due to waves. The AWS coupled with LPMSG can be modeled using the

Table 1: System nomenclature and values [16,25,37,39]

Symbol	Nomenclature	Value
$P_{PV}, P_{AWEC}, P_{BDDG}, P_{EV}$	Power output of solar PV, AWEC, BDDG, PHEV unit	–
P_{d1}, P_{d2}	Load demand (*p.u*)	–
K_{PV}	Gain of Solar PV unit	1
T_{PV}	Time constant of Solar PV unit	1.8 s
K_{AWEC}	Gain of AWEC unit	1
T_{AWEC}	Time constant of AWEC unit	0.3 s
K_{PE}	Gain of Power electronics unit	1
T_{PE}	Time constant of Power electronics unit	0.01 s
K_{VR}	Gain of valve actuator	1
T_{VR}	Time constatnt of valve actuator	0.05 s
K_{CE}	Gain of combustion engine unit	1
T_{CE}	Time constant of combustion engine unit	0.5 s
K_{EV}	Gain of PHEV unit	1
T_{EV}	Time constant of PHEV unit	0.2 s
T_H	Time constant of hydraulic amplifier	0.08 s
T_T	Time constant of turbine	0.3 s
K_r	Reheat gain	0.5
T_r	Reheat time constant	10 s
M_1, M_2	Moments of inertia	0.2, 0.166 s
D_1, D_2	Damping constants	0.012, 0.008 (p.u MW/Hz)
R_1, R_2	Primary control droop constants of area-1 and 2	2.4 (HZ/p.u MW)
B_1, B_2	Bias factors	0.429, 0.424
T_{D1}, T_{D2}	Communication delays	1.2, 1 s
T_{12}	Synchronizing Tie-Line Co-efficient	0.07

transfer function [41],

$$G_{AWEC} = \frac{K_{AWEC}}{1 + sT_{AWEC}} \tag{6}$$

2.3 Power Electronics Interface

The transfer function model of generator side converters and grid side inverters used to interface with the grid is approximated as [41],

$$G_{PE} = \frac{K_{PE}}{1 + sT_{PE}} \tag{7}$$

2.4 Bio-diesel Driven Generator (BDDG)

The output of RESs like Solar PV and AWEC is intermittent. Thus, a controllable generation system such as diesel engine generator is essential to provide reliable power to the loads. Bio-diesel is the product of the process of transesterification. It is renewable, bio-degradable,

non toxic, and can be produced from agricultural and plant resources. It can be compatible with conventional diesel and blended with it in any proportion. Thus, it can be operated in a conventional diesel engine [42].

The speed at which the BDDG does the mechanical work can be represented by [39,43],

$$\frac{dW}{d\theta} = \frac{\Re T V_{disp}}{2} \left(\frac{0.5 \sin 2\theta}{\sqrt{2(L/S)^2 - (\sin \theta)^2}} - \sin\theta \right) \tag{8}$$

where θ and T represent the angular movement measured from BDC in degree and the temperature at θ in kelvin, respectively. L and V_{disp} represent the connecting rod length in meter and displacement volume in m^3, respectively. S represents the stroke length in meters. $\Re = 8.314$ kJ/kmol K represents the universal gas constant.

The speed governor enabled with the control loop of regulation co-efficient R can be used to perform primary load frequency support by adjusting the valve actuator of the BDDG. The conventional diesel engine model can be used for the BDDG model. The transfer function of the valve actuator and combustion engine can be represented as follows [23],

Valve actuator dynamics [23],

$$G_{VR} = \frac{K_{VR}}{1 + sT_{VR}} \tag{9}$$

Combustion engine dynamics [23],

$$G_{CE} = \frac{K_{CE}}{1 + sT_{CE}} \tag{10}$$

$$G_{BDDG} = \left(\frac{K_{VR}}{1 + sT_{VR}} \right) \left(\frac{K_{CE}}{1 + sT_{CE}} \right) \tag{11}$$

2.5 Plug-in Hybrid Electric Vehicle

With the penetration of unpredictable RESs, the ESS, which stores the surplus renewable energy and supply for the demand whenever needed, is essential. In this regard, electric vehicle (EV), with its bidirectional connection capability of the converter, can be used as an ESS to absorb excess renewable energy and supply it to the grid whenever needed. The real power transfer between the battery of EVs and the power grid can be modeled using a differential equation. Thus, a first-order lag transfer function can be used for the frequency control model of PHEV, which can be represented as [44],

$$G_{EV} = \frac{K_{EV}}{1 + sT_{EV}} \tag{12}$$

2.6 Conventional Synchronous Generator

In our study, the CPP includes a thermal power plant of reheat type and is considered as the generating unit. The transfer function model of reheat-thermal power plant includes the hydraulic amplifier, reheat turbine model and can be represented as [16,17],

$$G_{TP} = \left(\frac{1}{1 + sT_H}\right) \left(\frac{1}{1 + sT_T}\right) \left(\frac{K_r T_r s + 1}{1 + sT_r}\right) \qquad (13)$$

2.7 Load and Machine Dynamics of VPP

The frequency deviations occur upon any power imbalance within the system. The net power imbalance at any instant in the independent area of VPP can be represented as,

$$\Delta P_e = (P_{PV} + P_{AWEC} + P_{BDDG} \pm P_{EV}) - P_{d1} \qquad (14)$$

The change in frequency due to change in net power is represented by the transfer function as follows [39],

$$G_{sys} = \frac{\Delta f}{\Delta P_e} = \frac{1}{Ms + D} \qquad (15)$$

The frequency got deviated based on the moments of inertia (M) of the rotating mass in the system and the damping coefficient of the loads (D) within the system.

2.8 Control and Communication Architecture of VPP

The significant difference in the frequency control strategy of the conventional multi-area power system model and the grid-tied VPP model is its control and communication infrastructure. In the case of the grid-tied VPP model, the centralized control concept is adopted, which highly depends on ICT [31,37]. In the centralized control concept, EMS measures the deviations of frequencies and the tie-line power flow at the point of coupling between CPP and VPP. The EMS generates and sends the ACE signal to the central controller of the virtual power plant located within the VPP through the communication network, which is primarily a Wide Area Network (WAN) [36].

The VPP controller regularly (at short time intervals) receives information about the operating state of DERs (*i.e.* real power output), which is located far away from each other. On the basis of data from all DERs and ACE signals from EMS, the generation output of each DER is decided, and the central controller generates the control signal.

This communication from the central controller of VPP to DERs is generally through the Local Area Network (LAN) [36]. Since DERs are widely distributed within the VPP, communication delays are unavoidable in this network. Thus, a single delay element is approximated for both sending and receiving signals and included in the control loop of the system. The communication delay e^{-sT_D} is represented by the Pade first-order approximation in the form of the transfer function as [37]:

$$e^{-sT_D} = \frac{\frac{-1}{2}sT_D + 1}{\frac{1}{2}sT_D + 1} \qquad (16)$$

3. METHODOLOGY

The objective problem formulation and the adopted control strategy for our analysis are illustrated in the following topics.

3.1 Selection of Controllers

Choosing a suitable controller is essential to obtain effective system responses for our system. The most widely employed controller for process control in industry is the PID Controller. [45]. As the system complexity increases, the search for a more reliable and flexible controller is needed. In this regard, we have employed FOPID controller for our system, and its dynamic performance is compared with conventional PI and PID controllers.

3.1.1 Background of FOPID Controller

The development of fractional calculus, which is the generalization of ordinary integration and differentiation to non-integer order, paves the way for implying additional flexibilities to the control action of conventional PID controller [46]. The FOPID controller has two more parameters (λ, μ) than the PID controller, which improves the controlled system's dynamic and steady-state performance. Specifically, the integral and derivative action with its non-integer order in the FOPID controller increases the system's stability and attenuates the high-frequency noise signals, respectively. FOPID controller is also proved to be more robust to plant uncertainties and load disturbances [45,46].

The transfer function equation of the FOPID controller is given by [47] (Figure 2),

$$TF_{FOPID} = (K_p + K_i/s^\lambda + K_d s^\mu) \qquad (17)$$

where λ and μ represent the order of integral and differential operators in the FOPID controller, respectively. When we set the orders $\lambda = 1$ and $\mu = 1$, the FOPID controller functionality is the same as the PID controller.
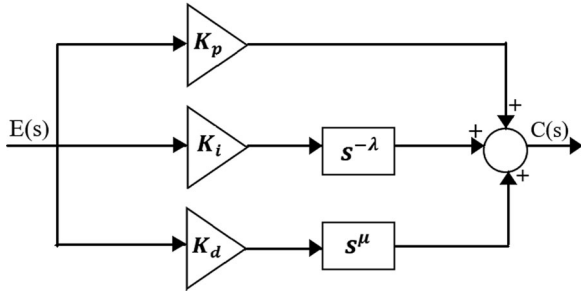
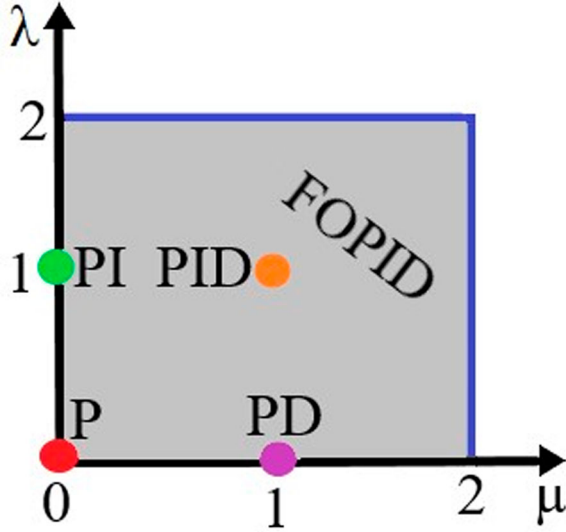**Figure 2:** Structure of FOPID controller

Figure 3: Plane representation of FOPID and PID controller

Thus FOPID controller can be regarded as the general case of conventional PID controller [45] (Figure 3).

The most commonly used definition for fractional order integral and differential operators is Riemann–Liouville (RL) definition and is presented as [47]:

$$aD_t^\alpha f(t) = \frac{1}{\Gamma(n-\alpha)} \frac{d^n}{dt^n} \int_a^t (t-\tau)^{n-\alpha-1} f(\tau) d\tau \qquad (18)$$

$$aD_t^{-\alpha} f(t) = \frac{1}{\Gamma(\alpha)} \frac{d^n}{dt^n} \int_a^t (t-\tau)^{\alpha-1} f(\tau) d\tau;$$

$$n-1 \geq \alpha > n. \qquad (19)$$

where $\Gamma(.)$ represents Euler's gamma function. aD_t^α and $a D_t^{-\alpha}$ represent the fractional order differentiation and integration, respectively. The Oustaloup recursive approximation is used to represent the fractional integro-differential operator in the frequency domain, which

represents a higher-order analog filter is [45],

$$s^\alpha = K \prod_{k=-N}^{N} \frac{s + \omega_k'}{s + \omega_k} \qquad (20)$$

where the poles, zeros, and gains can be calculated by [45],

$$\omega_k = \omega_b \left(\frac{\omega_h}{\omega_b}\right)^{(k+N+\frac{1+\alpha}{2})/(2N+1)} \qquad (21)$$

$$\omega_k' = \omega_b \left(\frac{\omega_h}{\omega_b}\right)^{(k+N+\frac{1-\alpha}{2})/(2N+1)} \qquad (22)$$

$$K = \omega_h^\alpha \qquad (23)$$

where α represents the order of integral and differential operators. $(2N+1)$ and (ω_b, ω_h) represent the filter order and ranges of frequency, respectively. In our work, we have implemented oustaloup approximation of fifth-order with the frequency range of $(10^{-3}, 10^3)$ using FOMCON toolbox [48] in Simulink.

3.2 Formulation of Objective Function

An objective function should be formulated to implement the optimization problem. The integral performance indices can be applied as a deciding parameter to assess the dynamic characteristics of the responses generated using various controllers. In this regard, Integral of Squared Error (ISE), Integral of time squared error (ITSE), Integral of absolute error (IAE), Integral of time absolute error (ITAE) have been widely used as the objective function to obtain the optimal gains of the controllers. ISE and ITAE are found to perform better in ALFC studies as they specifically minimize the overshoots and settling time, respectively [26]. The ISE index is effective in attenuating peak overshoots, undershoots, and significant errors [26]. In our study, the ISE of the frequency deviations of VPP, CPP, and tie-line power deviations is considered as our objective function (J), which is represented as follows [37]:

$$\text{Minimize } J_{ISE} = \int_0^{t_{sim}} \{(\Delta f_1)^2 + (\Delta f_2)^2 + (\Delta P_{tie})^2\}.dt \qquad (24)$$

It is subject to:

$$K_p^{min} \leq K_p \leq K_p^{max}$$

$$K_i^{min} \leq K_i \leq K_i^{max}$$

$$K_d^{min} \leq K_d \leq K_d^{max}$$

$$0 \leq \lambda \leq 2$$

$0 \leq \mu \leq 2$

where K_p, K_i, K_d, λ, μ are parameters of the FOPID controller and t_{sim} represents the simulation time range. The minimization is done using optimization techniques by which the optimal gains of the controller can be obtained.

3.3 Selection of Optimization Technique

In our study, the meta-heuristics optimization algorithms such as PSO [49], FA [50], GOA [51], ALO [52], SCA [53], and SSA [54] have been employed to minimize the objective function. The parameters adopted for different techniques are presented in Table 2. The comparative analysis presented in Figures 5(a–d) shows that the SSA provides minimal objective function values and better dynamic performances than other techniques. Thus, SSA technique is adopted to tune the gains of the controllers in our study.

Table 2: Optimization technique parameters

Optimization algorithm	Parameters
PSO	c1 = 2
	c2 = 2
	w = 1
	wdamp = 0.99
FA	Randomness (α) = 0.25
	Attractiveness (β) = 0.2
	Absorption coefficient (γ) = 0.5
ALO	Ratio I = 1 (at starting)
SCA	No algorithm-specific parameters
GOA	Cmax = 1
	Cmin = 0.00004
	f = 0.5
	L = 1.5
SSA	c2 = rand(0,1)
	c3 = rand(0,1)

3.3.1 Background of Salp Swarm Algorithm

Salps are a family of marine creatures called Salpidae. Its transparent body is formed like a barrel and it moves forward by pumping the water through the body, which is identical to the movement of jellyfish. Its swarming behavior, called the salp chain, is inspired to form SSA. Its swarming behavior aims to acquire better locomotion and to search for food in oceans [54]. The flowchart of SSA is presented in Figure 4.

The salp chain population is classified into two types. The salp present at first in the salp chain is termed as leader salp. The remaining salps in the salp chain are follower salps. The leader salp guides the swarm, and the follower salps follow each other. The behavior of the salp chain is mathematically modeled to implement it as an optimization technique. The location of salps is defined in an n-dimensional search space. The salp chain is assumed to
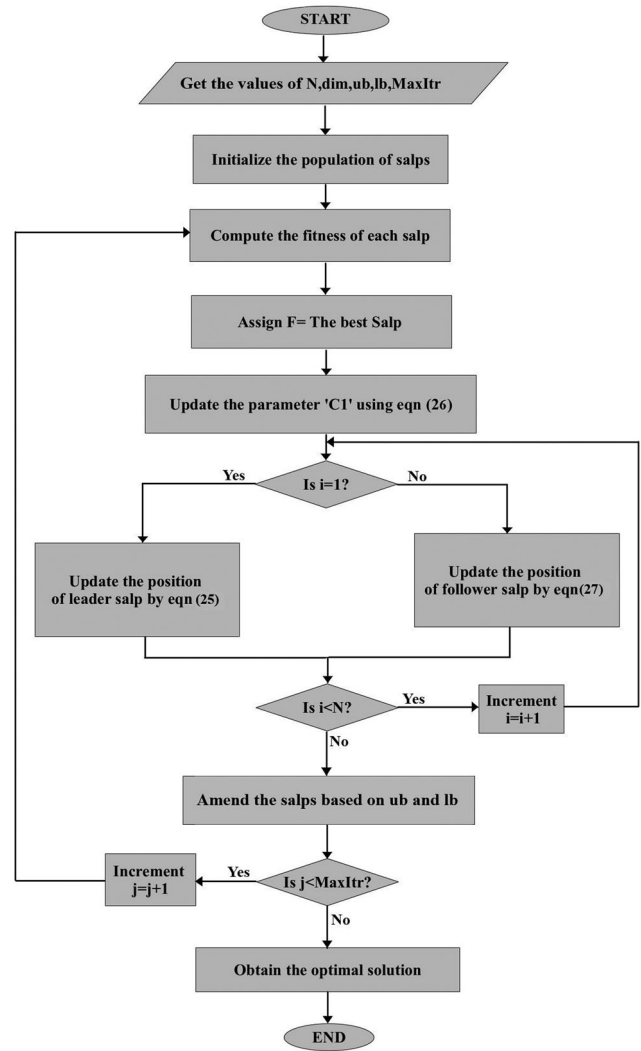
Figure 4: Flowchart of SSA technique

advance towards the target in order to reach the food supply target F (optimal solution). The movements of leader in the salp chain are defined by the following equation [54]:

$$x_j^1 = \begin{cases} F_j + C_1((ub_j - lb_j)C_2 + lb_j), & C_3 \geq 0 \\ F_j - C_1((ub_j - lb_j)C_2 + lb_j), & C_3 < 0 \end{cases} \quad (25)$$

where F_j indicates the food source position in j-th dimension, ub_j and lb_j denote the upper and lower bound in j-th dimension, respectively. x_j^1 indicates the position of leader salp in j-th dimension. C_2 and C_3 are the random numbers.

The parameter C_1 is the main controlling variable in SSA which balances the exploration and exploitation and is represented as [54],

$$C_1 = 2e^{-\left(\frac{4l}{L}\right)^2} \quad (26)$$

where l denotes the current iteration and L denotes the maximum iteration. The movements of followers in the salp chain are defined by the following equation [54],

$$x_j^i = \frac{1}{2}(x_j^i + x_j^{i-1}) \qquad (27)$$

where $i \geq 2$ and x_j^i indicates the position of i-th follower salp in the j-th dimension.

The main factors of SSA are [54]:

I. F is always given the best solution found so far, ensuring that it is never lost even if the swarm deteriorates.
II. The leader salp always exploits the search space and follows the food source.
III. The follower salps gradually follow the leading salp, by which they prevent SSA from trapping in local optima.
IV. The parameter C_1 decreases with iterations, by which the search space is first explored and then exploited (Figure 4).

## 4. SIMULATION RESULTS AND DISCUSSION

The proposed system is developed in MATLAB/SIMU-LINK R2021b environment. The Intel(R) Core(TM) i5-8265U, 1.80 GHz, 8GB RAM DELL laptop was used to run the simulations. The upper and lower bounds of the K_p, K_i, K_d parameters of the controllers are chosen between -1 and $+1$ obtained after exhaustive trials and errors. The fractional parameters λ and μ are chosen between 0 and 2. The simulations were performed for the maximum iteration of 200 to minimize J using optimization algorithms. The simulation time considered for each case is 120 s with a fixed step size of 0.001 s.

4.1 Case I: Performance Assessment of VPP System with PSO, FA, GOA, ALO, SCA, and SSA-tuned FOPID Controllers
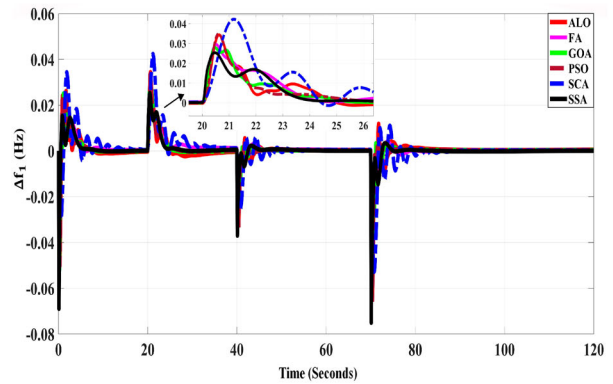
The Optimization techniques such as PSO, FA, GOA, ALO, SCA, and SSA are employed in FOPID controlled

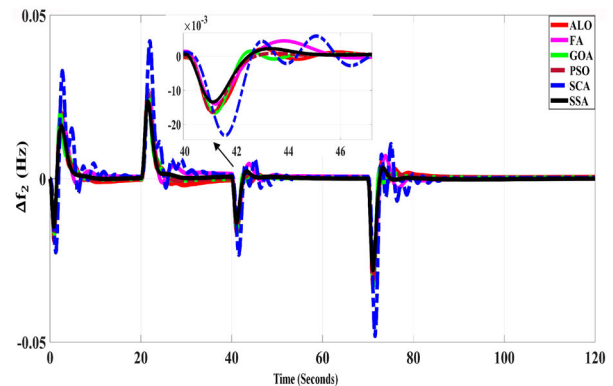**Table 3: Objective function values for different algorithms**

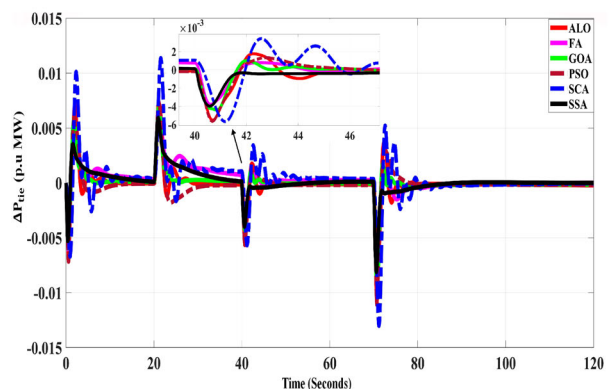| Optimization Technique	J_{ISE} (x 10^{-3})
ALO	7.58
FA	7.01
GOA	6.36
PSO	7.01
SCA	14.55
SSA	**5.63**
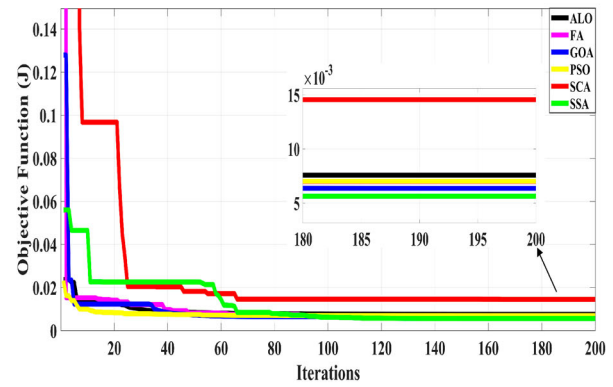
Figure 5: (a) Comparison of performance of ALO, FA, GOA, PSO, SCA, and SSA. (b) Δf_1 under different algorithms. (c) Δf_2 under different algorithms. (d): ΔP_{tie} under different algorithms

system to minimize the objective function J for the disturbances. Table 3 presents the obtained ISE values, and Figures 5) compares convergence curves obtained by each technique. From these results, it is clear that the SSA technique provides a minimal value of ISE error over the course of iterations.

The system responses $\Delta f_1, \Delta f_2, \Delta P_{tie}$, obtained using the different optimization algorithms are presented in Figure 5 (b–d), respectively. By comparative analysis, it is evident that the SSA technique can provide better system responses over other techniques for the disturbances as in Figure 6(a) in the system. In this regard, the SSA technique is chosen for tuning the controllers in our further studies.

4.2 Case II: Performance Assessment of VPP Model with FOPID, PID, and PI Controllers Tuned by Salp Swarm Algorithm

In this study, the FOPID, PID, and PI controllers are employed, and their dynamic performances under different scenarios of disturbances are analyzed. The SSA technique is used to obtain the optimal gains of the controllers. Figure 6) and Figure 7(a) represent two different load and generation scenarios in the system.
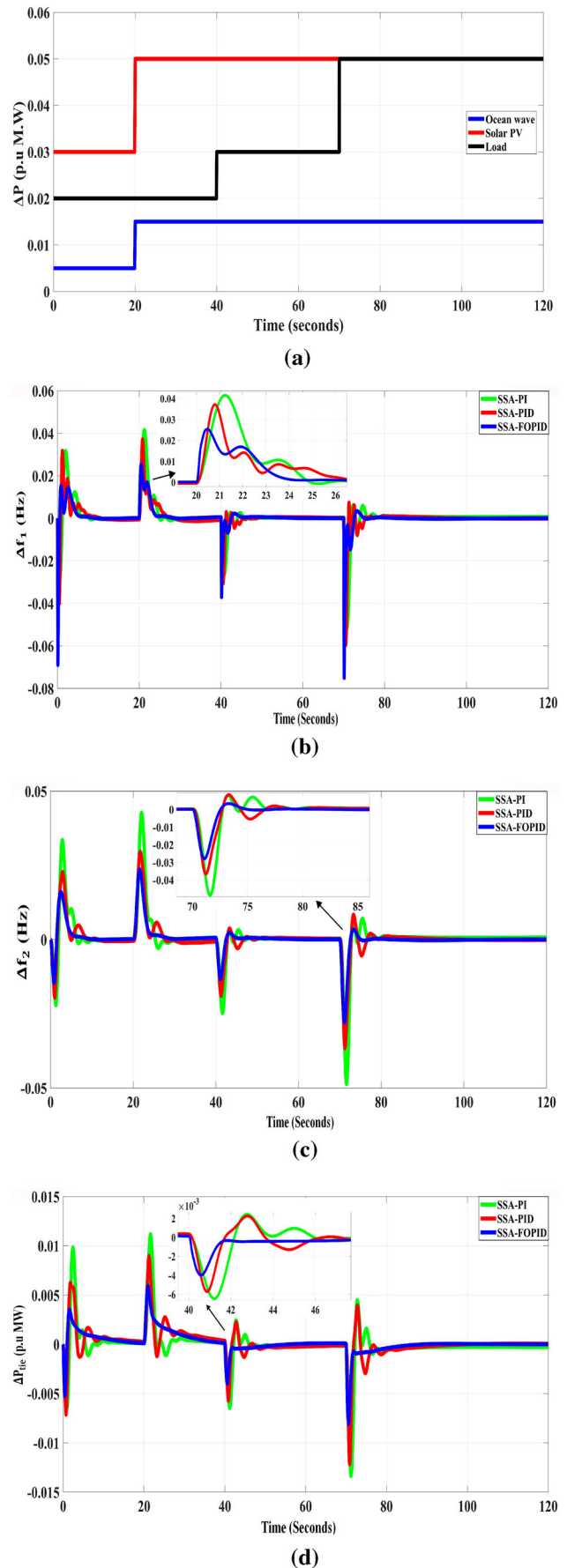
4.2.1 Scenario-I

Table 4: Decision parameters for scenario-I

	Dynamic characteristics	PI	PID	FOPID
Δf_1	Peak Overshoot (Hz)	0.040	0.037	**0.025**
	Peak Undershoot (Hz)	**0.046**	0.06	0.075
	Settling Time (sec)	75.38	74.9	**74.05**
Δf_2	Peak Overshoot (Hz)	0.042	0.029	**0.023**
	Peak Undershoot (Hz)	0.048	0.036	**0.028**
	Settling Time (sec)	76.34	76.14	**74.00**
ΔP_{tie}	Peak Overshoot (p.u)	0.011	0.008	**0.005**
	Peak Undershoot (p.u)	0.013	0.012	**0.008**
	Settling Time (sec)	73.33	75.31	**71.34**
Objective Function J(x 10^{-3})		14.44	9.17	**5.63**

4.2.2 Scenario-II

Figure 6(b–d) and Figure 7(b–d) show the system responses for scenario-I and II, respectively. Each plot compares the responses obtained using FOPID, PID, and PI controllers. The minimized ISE values for each controller and the dynamic characteristics obtained from the response plots $\Delta f_1, \Delta f_2, \Delta P_{tie}$ for both scenarios are presented in Tables 4 and 5. The results show that the SSA-tuned FOPID controllers provide the least values of the ISE function for both scenarios. It is also observed that the SSA-tuned FOPID controller provides better performances in terms of dynamic characteristics such as peak overshoot, peak undershoot, and settling time for

Figure 6: (a) Load and generation disturbance for scenario-I. (b) Δf_1 under FOPID, PID, PI controllers. (c) Δf_2 under FOPID, PID, PI controllers. (d) ΔP_{tie} under FOPID, PID, PI controllers

Table 5: Decision parameters for scenario-II

	Dynamic characteristics	PI	PID	FOPID
Δf_1	Peak Overshoot (Hz)	0.053	0.048	**0.035**
	Peak Undershoot (Hz)	**0.064**	0.074	0.079
	Settling Time (sec)	75.12	73.60	**72.26**
Δf_2	Peak Overshoot (Hz)	0.053	0.037	**0.034**
	Peak Undershoot (Hz)	0.060	0.046	**0.045**
	Settling Time (sec)	76.02	75.41	**73.71**
ΔP_{tie}	Peak Overshoot (p.u)	0.013	0.011	**0.008**
	Peak Undershoot (p.u)	0.016	0.015	**0.011**
	Settling Time (sec)	73.04	71.40	**71.19**
Objective Function J(x 10^{-3})		17.88	11.04	**7.56**

almost all the responses, except in the case of undershoot of Δf_1.

4.2.3 Scenario III: Absence of Renewable Energy Sources

In this case, the RESs such as Solar PV and Ocean wave energy sources are considered to be under maintenance or unavailable due to some adverse weather conditions. The step load disturbances of 1.5% from t = 0 to 20 s, then 4% from t = 20 to 70 s, and 3% from t = 70to 120 s as in scenario-II are simulated. Figure 8(a–c) shows the system's responses under certain conditions.

4.2.4 Scenario IV: Random Disturbances of Renewable Energy Sources

In this case, random disturbances of renewable sources as in Figure 9(a) are simulated to reflect certain extreme weather conditions. The responses of the system under these conditions are presented in Figure 9(b–d).

From the system responses of the studied cases in scenarios III and IV, it is clear that the overall performance of the SSA-tuned FOPID controller outperforms the PID and PI controller for our grid-tied VPP model.

4.3 Case III: Sensitivity Test of SSA-tuned FOPID Controllers Against System Uncertainties

4.3.1 Investigation of Robustness Against Load Uncertainties

To study the robustness of the FOPID-controlled system against load uncertainties, the disturbances as shown in Figure 6(a) are considered without resetting the controller's optimal gains. The system is studied under change in the loading condition up to ±25% of the nominal conditions.

It can be observed in Figure 10(a–c) that the responses due to the changes in load, almost follow the nominal load system responses but increase only in terms of undershoots for increased loads.
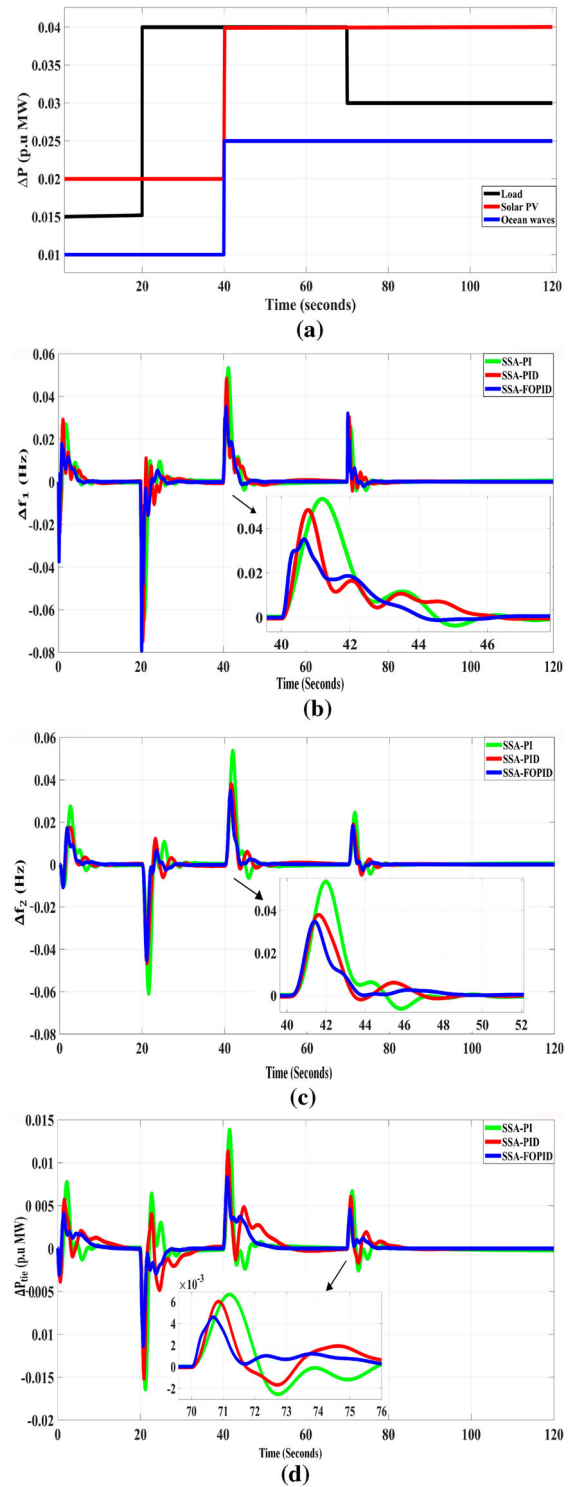
Figure 7: (a) Load and generation disturbance for scenario-II; (b) Δf_1 under FOPID, PID, PI controllers. (c) Δf_2 under FOPID, PID, PI controllers. (d) ΔP_{tie} under FOPID, PID, PI controllers

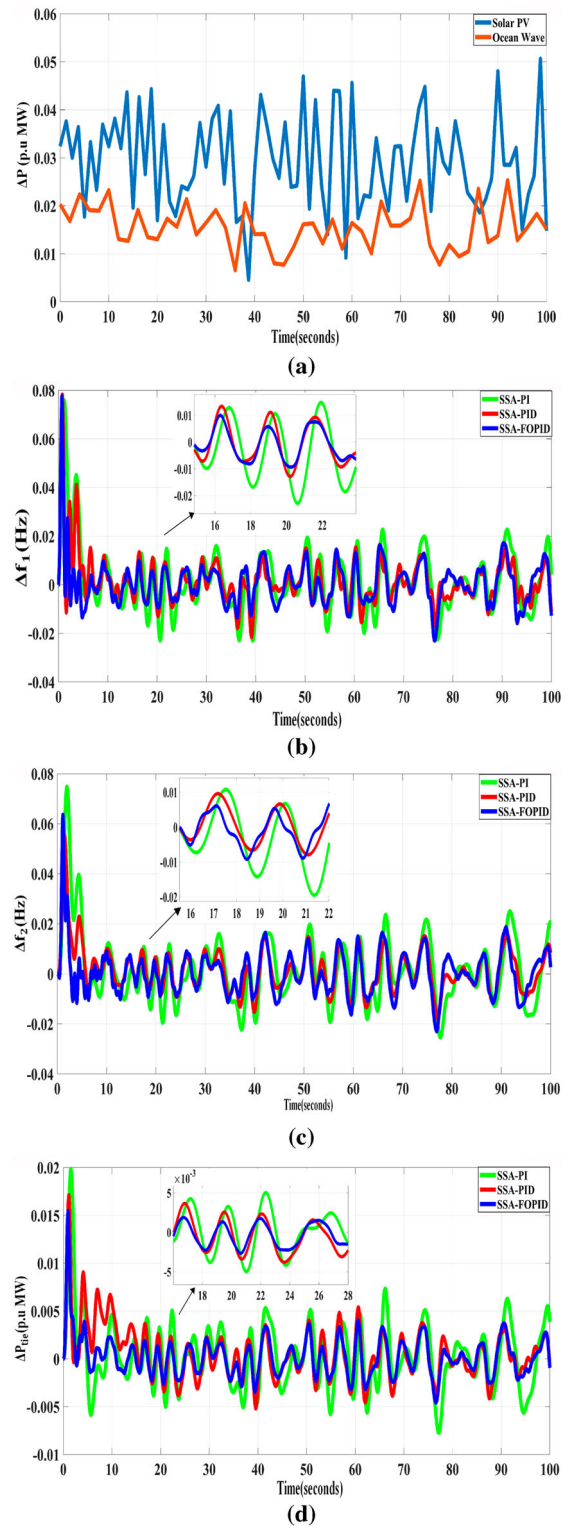### 4.3.2 Investigation of Robustness Against Synchronizing Tie-Line Coefficient (T12)

The robustness of the FOPID-controlled system against the Tie-Line Co-efficient (T12) parametric uncertainty is studied under the disturbances as in Figure 6(a). The
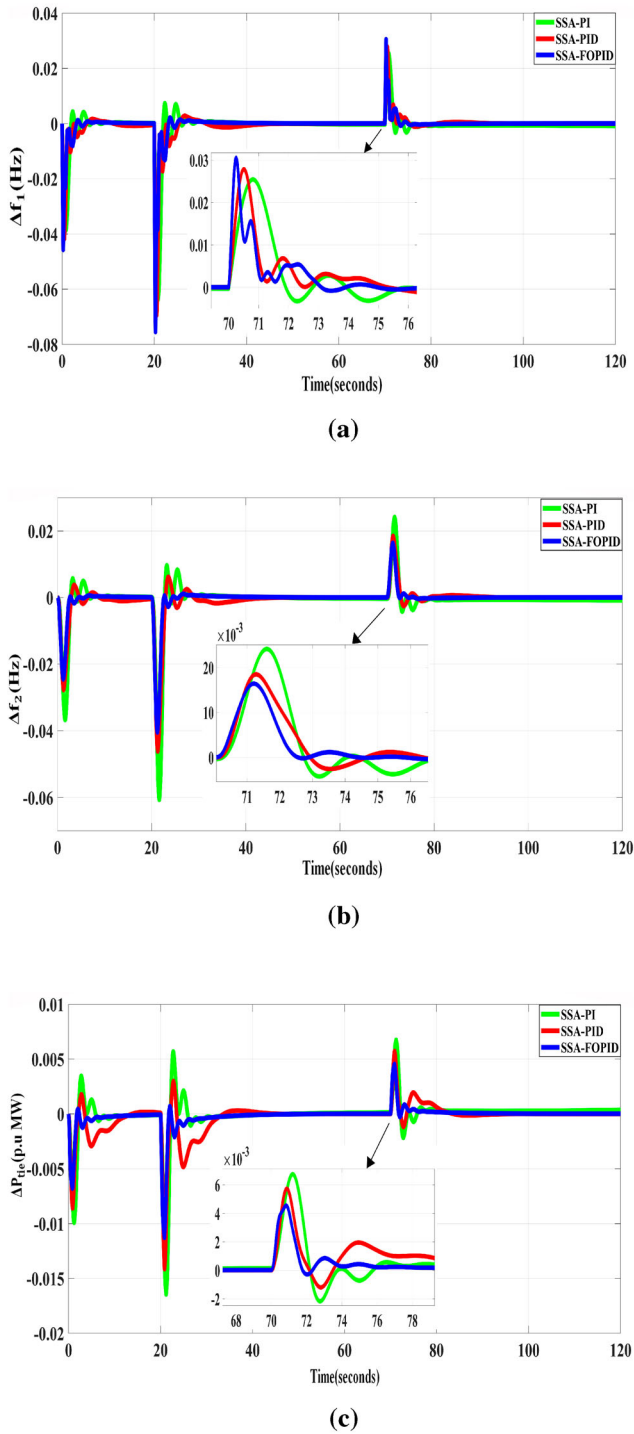
(a)

(b)

(c)

Figure 8: (a) Δf_1 under FOPID, PID, PI controllers. (b) Δf_2 under FOPID, PID, PI controllers. (c) ΔP_{tie} under FOPID, PID, PI controllers


(a)

(b)

(c)

(d)

Figure 9: (a): Random disturbances of Renewable sources (b) Δf_1 under FOPID, PID, PI controllers. (c) Δf_2 under FOPID, PID, PI controllers. (d) ΔP_{tie} under FOPID, PID, PI controllers

parameter T12 is considered to vary up to $\pm 20\%$ of its nominal values, keeping nominal controller gain values.

It is observed in Figure 11(a–c), that the variations in T12 do not have much effect on the system responses, and it retains almost the same responses as obtained under nominal conditions.

4.3.3 Investigation of Robustness Against Bias Factor (B2)

To study the sturdiness of the FOPID-controlled system against the Bias Factor (B2) parametric variations,
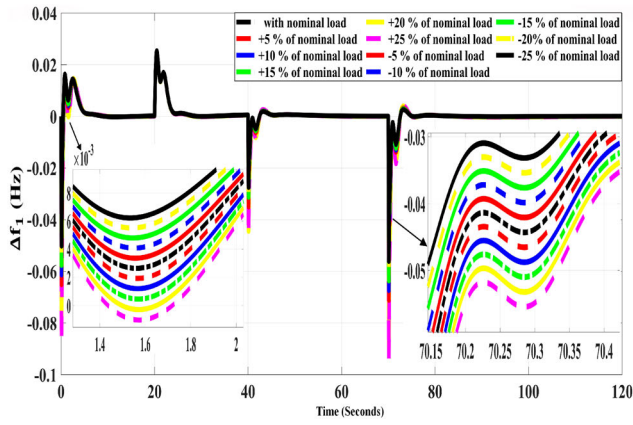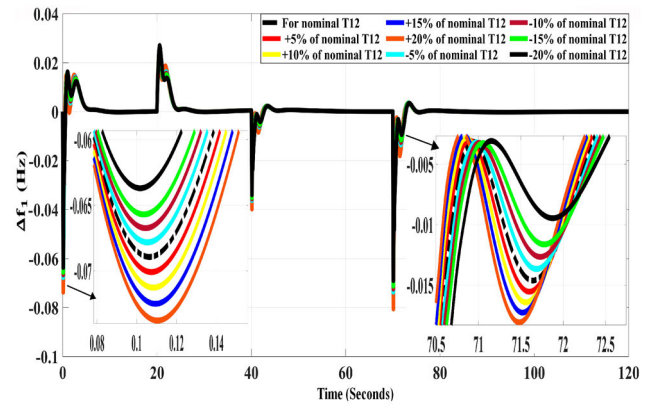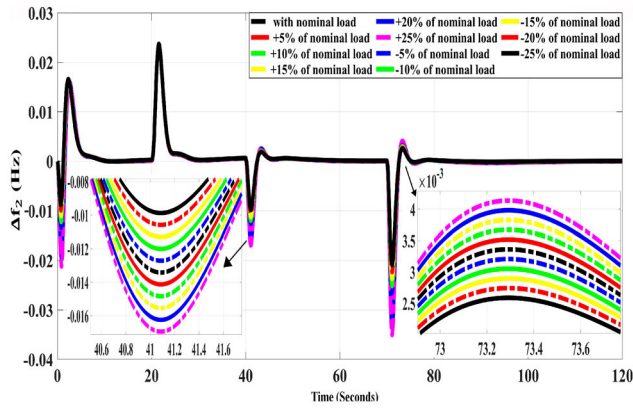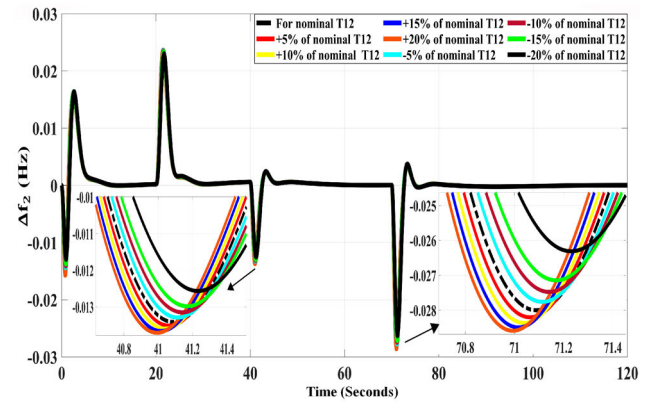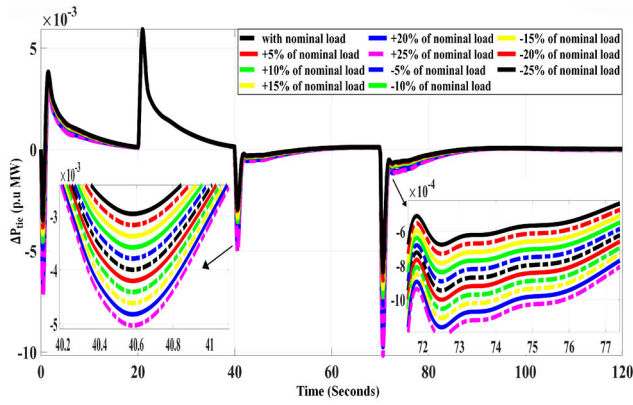
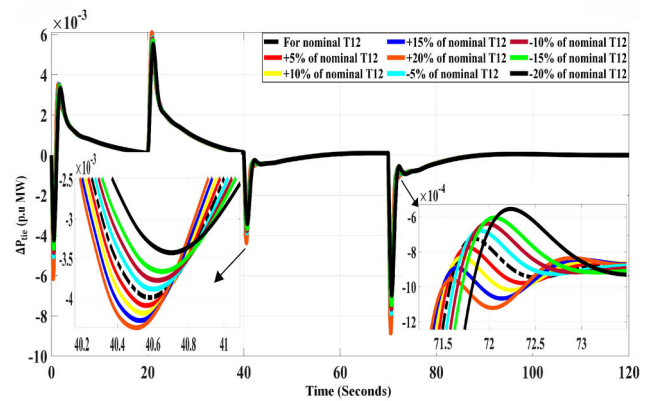**Figure 10:** (a) Δf_1 under load variations. (b) Δf_2 under load variations. (c) ΔP_{tie} under load variations

Figure 11: (a) Δf_1 under T12 variations. (b) Δf_2 under T12 variations. (c) ΔP_{tie} under T12 variations

the system responses are studied under varying B2 up to ±20% of its nominal value. It is observed in Figure 12(a–c) that the variations in B2 give the system responses almost the same as the nominal responses.

Thus, the overall sensitivity test results proved that the proposed SSA-tuned FOPID controller is robust against the load and parametric uncertainties for our grid-tied VPP system.

5. CONCLUSION

This work studied the frequency regulation of the grid-tied VPP with the structure of an independent control area of diverse DERs. Employing the VPP system with FOPID controller to analyze the system responses under disturbed conditions is a maiden attempt. The
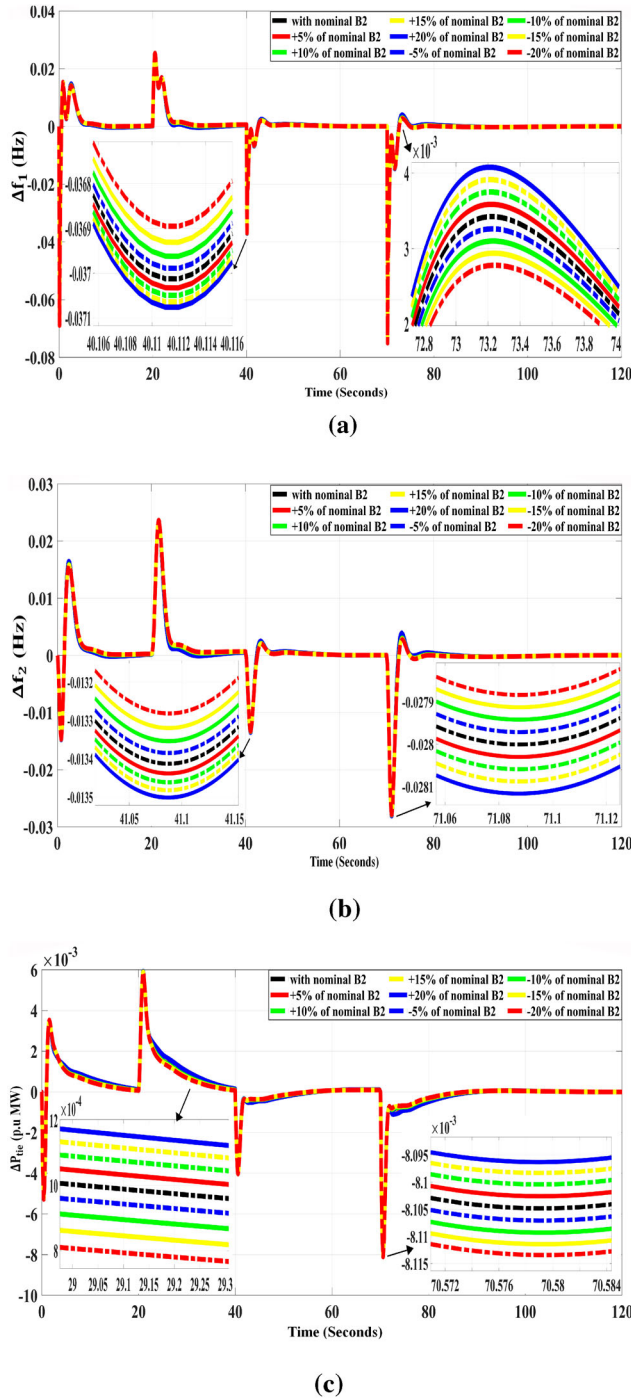
Figure 12: (a) Δf_1 under B2 variations. (b) Δf_2 under B2 variations. (c) ΔP_{tie} under T12 variations

conclusions drawn from the work are summarized as follows:

(1)   The solar PV-AWEC-BDDG-PHEV units in VPP and the conventional reheat-type thermal power plant have been mathematically modeled in the work.

(2)   The implemented algorithm SSA outperforms the other optimization algorithms in providing the ISE

value of 0.00563 which is lesser than the other techniques like PSO (0.00701), FA(0.00701), SCA (0.0145), ALO(0.00758) and GOA(0.00636). Thus, SSA is chosen to obtain the optimal gains of the controllers for our system.

(3)   In the first scenario of disturbances, the SSA-tuned FOPID controller is proved to provide a minimal ISE value (0.00563) than PID (0.00917) and PI controller (0.01444).

(4)   In the second scenario of disturbances, the SSA-tuned FOPID controller is proved to provide a minimal ISE value (0.00756) than PID (0.01104) and PI controller (0.01788).

(5)   Thus, the superiority of the SSA-tuned FOPID controller over PID and PI controller is realized after evaluating the time-domain specifications and ISE objective function values.

(6)   Finally, sensitivity analysis has been performed for the proposed SSA-tuned FOPID controlled system, taking into account the load and parametric uncertainties, and from the analysis, the robustness of the controller in withstanding the nominal responses against uncertainties is proved.

Hence, it can be concluded that the SSA-tuned fractional order PID controller is a better choice to sustain deviations upon any disturbances in the grid-tied VPP model.

In the future, modern controllers based control strategies can be adopted using advanced optimization techniques to improve the dynamic frequency response of the grid-integrated VPP model.

DISCLOSURE STATEMENT

No potential conflict of interest was reported by the author(s).

ORCID

Abishek R http://orcid.org/0000-0002-0893-5201
Dulal Chandra Das http://orcid.org/0000-0002-8161-3719
Ashtabhuj Kumar Srivastava http://orcid.org/0009-0002-5730-9941
Abdul Latif http://orcid.org/0000-0003-2851-7856

REFERENCES

1. O. I. Elgerd. "Electric energy systems theory: An introduction." 1982.

2. A. J. Wood, B. F. Wollenberg, and G. B. Sheblé. *Power Generation, Operation, and Control*. Hoboken, New Jersey: John Wiley & Sons, 2013.

3. P. Kundur, and Malik OP. *Power system stability and control.* New York: McGraw-Hill Education, 2022.

4. S. Heier. *Grid Integration of Wind Energy: Onshore and Off-shore Conversion Systems*. Hoboken: John Wiley & Sons, 2014.

5. J. P. Lopes, N. Hatziargyriou, J. Mutale, P. Djapic, and N. Jenkins, "Integrating distributed generation into electric power systems: A review of drivers, challenges and opportunities," *Electr. Power Syst. Res.*, Vol. 77, no. 9, pp. 1189–203, 2007.

6. T. Ackermann, G. Andersson, and L. Söder, "Distributed generation: A definition," *Electr. Power Syst. Res.*, Vol. 57, no. 3, pp. 195–204, 2001.

7. M. Lees, A. Collinson, and M. Barlow, "Practical measures to accommodate increased levels of distributed generation in existing distribution networks," in *Proceedings 17th International Conference on Electricity Distribution*, no. 32, 2003, pp. 12–15.

8. J. McDonald, "Adaptive intelligent power systems: Active distribution networks," *Energy. Policy.*, Vol. 36, no. 12, pp. 4346–51, 2008.

9. M. Braun, and P. Strauss, "A review on aggregation approaches of controllable distributed energy units in electrical power systems," *Int. J. Distrib. Energ. Res.*, Vol. 4, no. 4, pp. 297–319, 2008.

10. O. Palizban, K. Kauhaniemi, and J. M. Guerrero, "Microgrids in active network management – Part I: Hierarchical control, energy storage, virtual power plants, and market participation," *Renew. Sust. Energ. Rev.*, Vol. 36, pp. 428–39, 2014.

11. D. Pudjianto, C. Ramsay, and G. Strbac, "Virtual power plant and system integration of distributed energy resources," *IET Renew. Power Gener.*, Vol. 1, no. 1, pp. 10–16, 2007.

12. M. Braun, "Technological control capabilities of DER to provide future ancillary services," *Int. J Distrib. Energ. Res.*, Vol. 3, no. 3, pp. 191–206, 2007.

13. D. Pudjianto, C. Ramsay, and G. Strbac, "Microgrids and virtual power plants: Concepts to support the integration of distributed energy resources," *Proceed Institut. Mechan. Eng., Part A: J. Pow. Energ.*, Vol. 222, no. 7, pp. 731–741, 2008.

14. T. L. Vandoorn, B. Zwaenepoel, J. D. De Kooning, B. Meersman, and L. Vandevelde, "Smart microgrids and virtual power plants in a hierarchical control structure," in *2011 2nd IEEE PES International Conference and Exhibition on Innovative Smart Grid Technologies*, 2011, pp. 1–7. IEEE

15. R. N. Rao, and P. Rama Krishna Reddy, "PSO based tuning of PID controller for a load frequency control in two area power system," *Int. Eng. Res. Appl. (IJERA)*, Vol. 1.3, pp. 1499–505, 2015.

16. H. Gozde, M. Cengiz Taplamacioglu, and I. Kocaarslan, "Comparative performance analysis of artificial Bee Colony algorithm in automatic generation control for interconnected reheat thermal power system," *Int. J. Electr. Power Energy Syst.*, Vol. 42, no. 1, pp. 167–78, 2012.

17. A. K. Barisal, "Comparative performance analysis of teaching learning based optimization for automatic load frequency control of multi-source power systems," *Int. J. Electr. Power Energy Syst.*, Vol. 66, pp. 67–77, 2015.

18. M. A. El-Hameed, and A. A. El-Fergany, "Water cycle algorithm-based load frequency controller for interconnected power systems comprising non-linearity," *IET. Gener. Transm. Distrib.*, Vol. 10, no. 15, pp. 3950–61, 2016.

19. G. Mallesham, S. Mishra, and A. N. Jha, "Maiden application of Ziegler-Nichols method to AGC of distributed generation system," in *2009 IEEE/PES Power Systems Conference and Exposition*, 2009, pp. 1–7. doi:10.1109/PSCE.2009 .4840262.

20. D. C. Das, A. K. Roy, and N. Sinha, "GA based frequency controller for solar thermal–diesel–wind hybrid energy generation/energy storage system," *Int. J. Electr. Power Energy Syst.*, Vol. 43, no. 1, pp. 262–79, 2012.

21. R. H. Kumar, and S. Ushakumari, "Biogeography based tuning of PID controllers for load frequency control in microgrid," in *2014 International Conference on Circuits, Power and Computing Technologies [ICCPCT-2014]*. IEEE, 2014.

22. V. P. Singh, S. R. Mohanty, N. Kishor, and P. K. Ray, "Robust H-infinity load frequency control in hybrid distributed generation system," *Int. J. Electr. Power Energy Syst.*, Vol. 46, pp. 294–305, 2013.

23. A. A. l-Fergany, and M. A. El-Hameed, "Efficient frequency controllers for autonomous two-area hybrid microgrid system using social-spider optimiser," *IET. Gener. Transm. Distrib.*, Vol. 11, no. 3, pp. 637–48, 2017.

24. R. Khan, N. Gogoi, J. Barman, A. Latif, and D. C. Das, "Virtual power plant enabled co-ordinated frequency control of a grid connected independent hybrid microgrid using Firefly algorithm, pp. 795–800, 2019.

25. A. Latif, D. C. Das, A. K. Barik, and S. Ranjan, "Maiden coordinated load frequency control strategy for ST-AWEC-GEC-BDDG-based independent three-area interconnected microgrid system with the combined effect of diverse energy storage and DC link using BOA-optimised PFOID controller," *IET Renew. Power Gener.*, Vol. 13, no. 14, pp. 2634–46, 2019.

26. G. Shankar, and V. Mukherjee, "Load frequency control of an autonomous hybrid power system by quasi-oppositional harmony search algorithm," *Int. J. Electr. Power Energy Syst.*, Vol. 78, pp. 715–34, 2016.

27. D. L. de Souza, M. O. Oliveira, J. J. Gimenez Ledesma, and O. H. Ando Junior, "The virtual power plant for

the management and control of distributed generation – review," *Int. J. Adv. Eng. Res. Sci. (IJAERS)*, Vol. 6, pp. 458–65, 2019.

28. H. Saboori, M. Mohammadi, and R. Taghe, "Virtual power plant (VPP), definition, concept, components and types," in *2011 Asia-Pacific Power and Energy Engineering Conference*, 2011, IEEE, pp. 1–4.

29. G. Zhang, C. Jiang, and X. Wang, "Comprehensive review on structure and operation of virtual power plant in electrical system," *IET. Gener. Transm. Distrib.*, Vol. 13, no. 2, pp. 145–56, 2019.

30. D. Pudjianto, C. Ramsay, and G. Strbac, "Virtual power plant and system integration of distributed energy resources," *IET Renew. Power Gener.*, Vol. 1, no. 1, pp. 10–16, 2007.

31. W. Zhong, J. Chen, and M. Liu, "Mohammed Ahsan Adib Murad, and Federico Milano. "Coordinated control of virtual power plants to improve power system short-term dynamics," *Energies*, Vol. 14, no. 4, pp. 1182, 2021.

32. H. H. Alhelou, P. Siano, M. Tipaldi, R. Iervolino, and F. Mahfoud, "Primary frequency response improvement in interconnected power systems using electric vehicle virtual power plants," *World Elect. Vehicle J.*, Vol. 11, no. 2, pp. 40, 2020.

33. R. A. Ahangar, and A. Sheykholeslami, "Bulk virtual power plant, a novel concept for improving frequency control and stability in presence of large scale RES," *Int. J. Mechatronic., Electric. Comp. Techn.*, Vol. 4, no. 10, pp. 1017–1044, 2014.

34. W. Zhong, "Mohammed Ahsan Adib Murad, Muyang Liu, and Federico Milano. "Impact of virtual power plants on power system short-term transient response.","" *Electr. Power Syst. Res.*, Vol. 189, pp. 106609, 2020.

35. W. Zhong, T. Kërçi, and F. Milano. "On the impact of topology on the primary frequency control of virtual power plants." In 2021 *IEEE Madrid PowerTech*, pp. 1-6. IEEE, 2021.

36. L. Yuxuan, Z. Dongsheng, and T. Xisheng, "AGC control model of virtual power plant considering communication delay," in *2019 14th IEEE Conference on Industrial Electronics and Applications (ICIEA)*, 2019, IEEE, pp. 638–43.

37. P. P. Dey, D. C. Das, A. Latif, S. M. Hussain, and T. S. Ustun, "Active power management of virtual power plant under penetration of central receiver solar thermal-wind using butterfly optimization technique," *Sustainability*, Vol. 12, no. 17, pp. 6979, 2020.

38. A. K. Srivastava, A. Latif, S. C. Shaoo, D. C. Das, S. M. Suhail Hussain, and T. S. Ustun, "Analysis of GOA optimized two-stage controller for frequency regulation of grid integrated virtual power plant," *Energy Reports*, Vol. 8, pp. 493–500, 2022.

39. A. K. Barik, and D. C. Das, "Expeditious frequency control of solar photovoltaic/biogas/biodiesel generator based isolated renewable microgrid using grasshopper optimisation algorithm," *IET Renew. Power Gener.*, Vol. 12, no. 14, pp. 1659–67, 2018.

40. H. M. Hasanien, "Gravitational search algorithm-based optimal control of archimedes wave swing-based wave energy conversion system supplying a DC microgrid under uncertain dynamics," *IET Renew. Power Gener.*, Vol. 11, no. 6, pp. 763–70, 2017.

41. H. M. Hasanien, "Whale optimisation algorithm for automatic generation control of interconnected modern power systems including renewable energy sources," *IET. Gener. Transm. Distrib.*, Vol. 12, no. 3, pp. 607–14, 2018.

42. A. K. Agarwal, "Biofuels (alcohols and biodiesel) applications as fuels for internal combustion engines," *Prog. Energy Combust. Sci.*, Vol. 33, no. 3, pp. 233–71, 2007.

43. A. S. Ramadhas, S. Jayaraj, and C. Muraleedharan, "Theoretical modeling and experimental studies on biodiesel-fueled engine," *Renewable Energy*, Vol. 31, no. 11, pp. 1813–26, 2006.

44. R. Khezri, A. Oshnoei, M. T. Hagh, and S. M. Muyeen, "Coordination of heat pumps, electric vehicles and AGC for efficient LFC in a smart hybrid power system via SCA-based optimized FOPID controllers," *Energies*, Vol. 11, no. 2, pp. 420, 2018.

45. I. Tejado, B. M. Vinagre, J. E. Traver, J. Prieto-Arranz, and C. Nuevo-Gallardo, "Back to basics: Meaning of the parameters of fractional order PID controllers," *Mathematics*, Vol. 7, no. 6, pp. 530, 2019.

46. C. A. Monje, Y. Chen, B. M. Vinagre, D. Xue, and V. Feliu-Batlle. *Fractional-order Systems and Controls: Fundamentals and Applications*. London: Springer Science & Business Media, 2010.

47. I. Podlubny, "Fractional Differential Equations: An Introduction to Fractional Derivatives, Fractional Differential Equations, to Methods of Their Solution and Some of Their Applications," *Math. Sci. Eng*, Vol. 198, pp. 340, 1999.

48. A. Tepljakov, E. Petlenkov, and J. Belikov, "FOMCOM: A MATLAB toolbox for fractional-order system identification and control," *Int. J. Microelectron Comp. Sci.*, Vol. 2, no. 2, pp. 51–62, 2011.

49. J. Kennedy, and R. Eberhart, "Particle swarm optimization," in *Proceedings of ICNN'95-International Conference on Neural Networks*, vol. 4, 1995, IEEE pp. 1942–8.

50. X.-S. Yang, "Firefly algorithm, stochastic test functions and design optimisation," *Int J Bio-Inspir Comp*, Vol. 2, no. 2, pp. 78–84, 2010.

51. S. Saremi, S. Mirjalili, and A. Lewis, "Grasshopper opti-
misation algorithm: Theory and application," *Adv. Eng.
Softw.*, Vol. 105, pp. 30–47, 2017.

52. S. Mirjalili, "The ant lion optimizer," *Adv. Eng. Softw.*,
Vol. 83, pp. 80–98, 2015.

53. S. Mirjalili, "SCA: A sine cosine algorithm for solv-
ing optimization problems," *Knowl. Based. Syst.*, Vol. 96,
pp. 120–33, 2016.

54. S. Mirjalili, A. H. Gandomi, S. Z. Mirjalili, S. Saremi, H.
Faris, and S. M. Mirjalili, "Salp swarm algorithm: A bio-
inspired optimizer for engineering design problems," *Adv.
Eng. Softw.*, Vol. 114, pp. 163–91, 2017.

AUTHORS

Abishek R received his B E degree in electrical and electronics engineering from Government College of Technology, Coimbatore, Tamilnadu in 2019. Currently, he is pursuing his MTech degree in power and energy systems engineering from the Department of Electrical Engineering, National Institute of Technology Silchar, Assam. His research interests include distributed generation, modeling and control of renewable energy systems, virtual power plant and load frequency control.

Corresponding author. Email: abi210498@gmail.com

Dulal Chandra Das received his PhD degree in electrical engineering from the National Institute of Technology Silchar, Assam in 2014. Currently, he is working as an assistant professor at the Department of Electrical Engineering, National Institute of Technology Silchar, Assam. His research interests are demand side management, renewable energy technologies, energy storage devices and application of soft computing techniques in renewable-based hybrid energy systems for its operation and control.

Email: dulal_nit@yahoo.co.in

Ashtabhuj Kumar Srivastava received his BTech degree in electrical and electronics engineering from IMS Engineering College, Ghaziabad, Uttar Pradesh in 2016. He received his MTech degree in power and energy systems engineering from the Department of Electrical Engineering, National Institute of Technology Silchar, Assam in 2021. Currently, he is pursuing his PhD degree in electrical engineering from the Indian Institute of Technology Roorkee, Uttarakhand. His area of research includes Solar energy, microgrid, and renewable energy systems.

Email: ashtabhujsri143@gmail.com

Abdul Latif received his BTech degree in electrical engineering from Aliah University, in 2014. He received his MTech degree in electrical engineering from the National Institute of Technology Agartala in 2016 and completed his PhD degree in electrical engineering from the Department of Electrical engineering, National Institute of Technology Silchar in 2021. Currently, he is working as a post doctoral research associate at Khalifa University, UAE. His research interests include modeling and control of frequency response renewable microgrid system, automatic power-frequency management, frequency response virtual power plant, and smart grid.

Email: abdul.latif@ku.ac.ae